

**COB-2019-1524**  
**NUMERICAL ANALYSIS OF THE SWEEP BLADES EFFECT ON THE  
AERODYNAMIC PERFORMANCE OF AXIAL FANS**

Tania M. A. Angulo, [tani.arispe@unifei.edu.br](mailto:tani.arispe@unifei.edu.br)

Ramiro G. R. Camacho, [ramirez@unifei.edu.br](mailto:ramirez@unifei.edu.br)

Waldir de Oliveira, [waldir@unifei.edu.br](mailto:waldir@unifei.edu.br)

Edna R. da Silva, [ednaunifei@yahoo.com.br](mailto:ednaunifei@yahoo.com.br)

Germán E. Niño Del Río, [ge.nino@hotmail.com](mailto:ge.nino@hotmail.com)

Federal university of Itajubá, Av. BPS, 1303, Bairro Pinheirinho, Itajubá - MG - Brasil. 37500 903

**Abstract.** *The sweep forward in axial flow fan blades, which consists of a tangential displacement in the direction of rotor rotation, has proved to have several advantages in aerodynamic performance. Some of the sweep advantages in axial fan blades are the increased in efficiency and total pressure variation, compared to non-swept blades or shaped curved blades in arc of circle format. The motivation of this research is the analysis through Computational Fluid Dynamics, of the aerodynamic performance, considering different configurations of forward swept blades of axial fans. In this sense, the present work presents the numerical study of fans rotor with swept blades, designed from the operational data of a shaped flat curved blades fan. Different swept blade fan configurations are generated, based on cubic functions that define the center line of the blade, taken at 50% of the leading edge of each blade airfoil. According to the aerodynamic performance analysis, it is evidenced that the fans with swept blades present high efficiency for a wide flow rate. Being that those fans with sweep in the blades most accentuated in the tip, present a better aerodynamic performance.*

**Keywords:** Axial fan, Aerodynamic, Computational Fluid Dynamics, Sweep.

## 1. INTRODUCTION

Axial fans are used in many industrial applications, where medium and high efficiency rotor designs can be developed for each application. Nowadays, several design methodologies have been applied, in order to obtain axial fans more robust and efficient. One technique to improve the rotor axial aerodynamic performance is the Sweep, which consists of the rotor blades displacement in the tangential direction. The sweep has the purpose to reduce flow losses and, consequently, increase the efficiency of the axial flow rotors.

In the studies of Ohtsuta & Akishita (1990), Kwedikha (2009) and VAD (2011), comparative studies of axial fan rotors with forward swept and backward swept were carried out. Forward sweep is a displacement of the rotor blades in a tangential direction in the sense of rotor rotation, and a backward sweep is a displacement of the rotor blades in a tangential direction in the opposite sense to a rotor direction of rotation. See Figure 1.

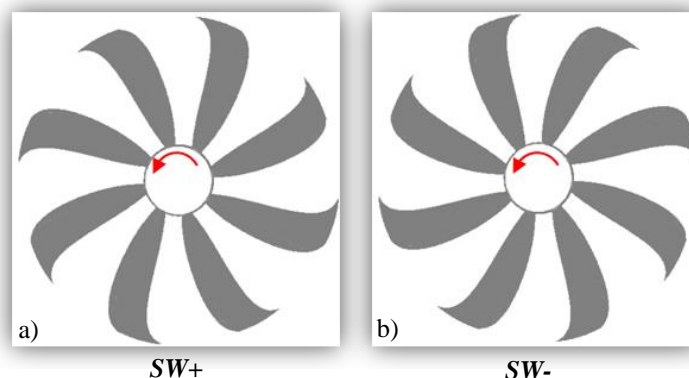


Figure 1. Sweep axial flow fan. a) forward sweep, b) backward sweep.

It has been shown that advantages in aerodynamic performance of the blades with forward sweep (in the direction of rotor rotation) are higher compared with the backward sweep blades (contrary to the rotor rotation direction). The reason is that with the forward sweep, low momentum fluid particles in the blade boundary layer have to travel a shorter distance before they reach the trailing edge and thus induce smaller losses.

Some advantages of forward sweep blades fans are the wide range of volumetric flow and increased pressure in the fan duty region (Wright & Simmons, 1989).

Due to sweep advantages, the fan literature suggests some methods that allow sweep to be included in the preliminary design (Masi et al., 2018). This article presents the axial fans aerodynamic performance; obtained from numerical simulations using Computational Fluid Dynamics techniques. Different models were considered: a fan of flat curved blades; and 9 sweep fan geometries, designed from the point of maximum efficiency of the fan of flat curved blades. To quantify the forward sweep effects in the rotor blades of the fans, behavioral curves relating to the variation of total pressure, hydraulic power and the efficiency of the 10 fans are compared.

For the development of the aerodynamic design of the axial rotors analyzed in this work, the forward sweep was considered.

## 2. STUDY CASES DESCRIPTION

In this work 10 axial flow fan rotors are analyzed. The first case study is a curved flat blade fan rotor, VPC, with outside diameter,  $D_e = 500$  mm, hub ratio,  $\nu = Di/De = 0,14$  and numbers of blades,  $N=8$ .

From the operating conditions of the VPC axial fan rotor, an axial rotor was designed based on the lift wing theory (Albuquerque, 2006) for the free vortex condition. The designed axial flow rotor has been modified resulting in 9 forward sweep blade rotors. These rotors were coded by  $Sw1$ ,  $Sw2$ ,  $Sw3$ ,  $Sw4$ ,  $Sw5$ ,  $Sw6$ ,  $Sw7$ ,  $Sw73$  e  $Sw7310$ , characterizing the various studied geometries.

The fan rotor geometries  $Sw1$ ,  $Sw2$ , ... e  $Sw7310$ , were obtained through variations in the chord,  $la$ , and the blade thickness,  $e_{max}$ , hub ratio,  $\nu$ , and cubic functions that define the center line of the blade, taken at 50% of the leading edge of each blade profile.

The cubic functions are a function of the following quantities:

- The sweep angle,  $\gamma$ , which defines the counterclockwise rotation of the blade tip from the point  $e$ , to point  $e^*$ ;
- The angles  $\delta_i$  and  $\delta_e$  formed between the ordinate  $x$  and the tangents to the points  $i$  and  $e^*$ , respectively.

Thus, the cubic function considered to generate sweep blades is expressed according to Eq. (1).

$$f(x) = y = ax^3 + bx^2 + cx + d \quad (1)$$

With:  $a, b, c, d = f(\lambda, \delta_e, \delta_i, \nu)$

The angles that result in the geometry of the sweep blades are shown in Figure 2.

In Table I, the geometric characteristics of the 9 geometries of swept blades fans are presented.

Table I. Geometric Variations of sweep fans

FAN	$\lambda$	$\delta_i$	$\delta_e$	Di/De	Note
VPS1	15°	100°	120°	0,21	Chord and thickness varying from base to tip blade.
VPS2	25°	115°	150°	0,21	
VPS3	20°	100°	180°	0,21	
VPS4	20°	100°	180°	0,21	No variation of chord and thickness
VPS5	20°	100°	180°	0,24	
VPS6	20°	100°	180°	0,24	
VPS7	20°	100°	180°	0,24	No variation of chord; but $e_{base} > e_{tip}$
VPS73	20°	100°	180°	0,24	
VPS7310	20°	100°	180°	0,24	Chord and thickness varying from base to tip blade.

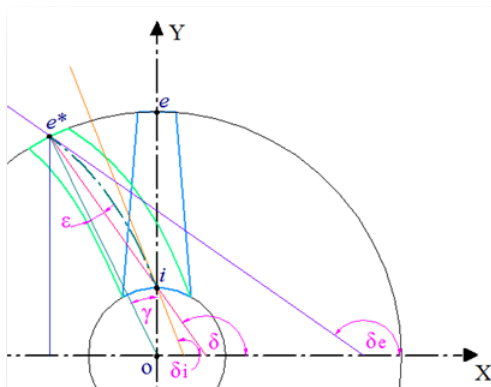


Figure 2. Geometric parameterization for sweep variations.

Thus, in  $Sw1$  geometry, the displacement is smooth, moderate and uniform. In  $Sw2$  geometry, the displacement is more pronounced making the displacement of the tip profile from the blade base profile more pronounced. In the  $Sw3$ ,

$Sw4$ ,  $Sw5$ ,  $Sw6$ ,  $Sw7$ ,  $Sw73$  e  $Sw7310$  geometries, displacement despite being a smooth displacement, is variable from the base to the tip, being the region closest to the tip of the blade being more accelerated due to the cubic function, which is more pronounced in this region.

### 3. NUMERICAL SIMULATION

For the numerical simulation of the flow field, it was considered a steady, incompressible and isothermal flow. The density and the dynamic viscosity used in the numerical simulations were:  $\rho = 1,225 \text{ kg/m}^3$  e  $\mu = 1,7894e-5 \text{ kg/m.s}$ , respectively.

For the calculation of the local flow field, the commercial program Fluent<sup>®</sup> was used, which solves the conservation equations of mass and momentum for the discretized domain. For the computational simulation the turbulence model  $k-\omega/SST$  was used.

#### 3.1 Computational mesh generation

Both the geometry modeling and the computational mesh generation were performed in the ICEM CFD<sup>®</sup> commercial program.

For the fan simulations, two domains were considered: the domain corresponding to the complete rotor, and an output domain. The domain is cylindrical from the rotor input to the output surface and comprises extending the rotor hub. With this approach it can be accurately predict the aerodynamic behavior of the axial rotor, with the advantage of having a smaller size domain (Augustyn, 2013).

Figure 3 presents the computational domain considered for the simulations of the both axial flow rotors: the curved flat blade rotor, VPC, and blade rotors with sweep.

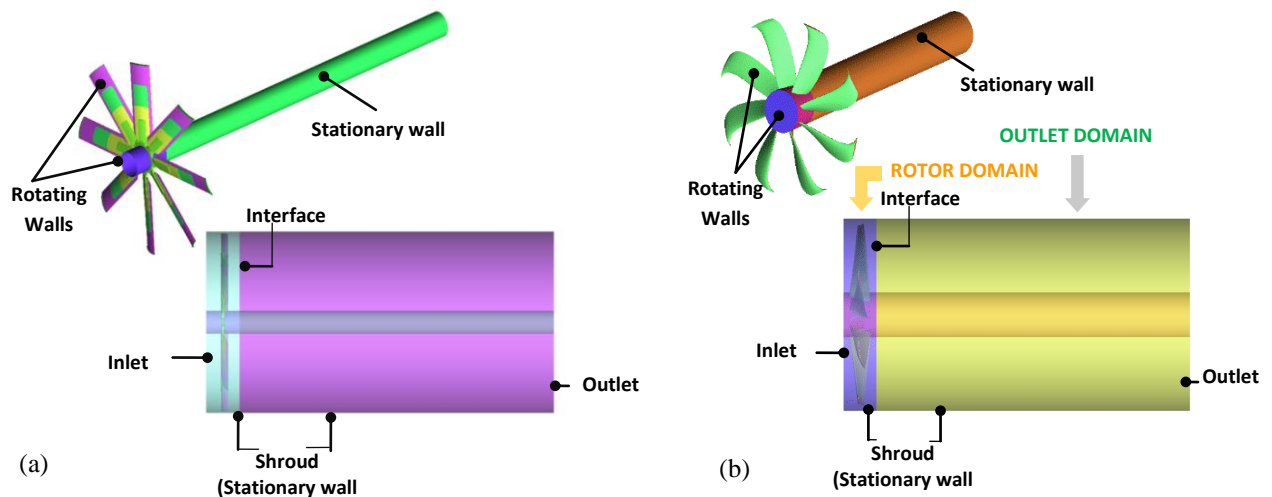


Figure 3. Computational domain and boundary conditions. (a) VPC axial flow fan, (b) Sweep axial flow fan.

In the rotor domain, a non-structured hybrid mesh with tetrahedral elements, hexahedral nucleus and prismatic layer was used in the blade regions.

For the output domain, a hexahedral mesh was considered. Figure 4 shows the meshes of the axial flow rotor blades of curved flat blades and sweep blades, respectively. Figure 5 shows the detail of mesh refinement in the blades of both rotors.

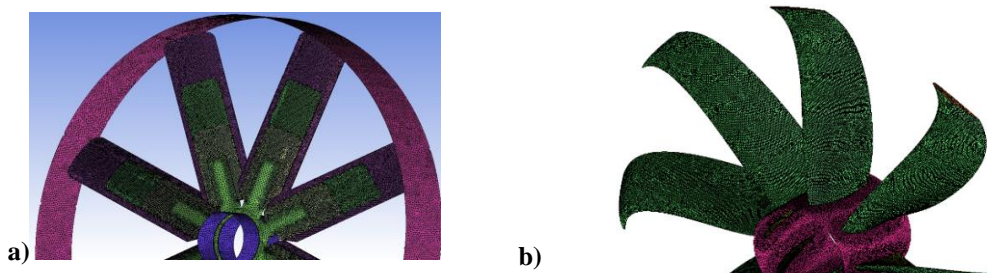


Figure 4. Tetrahedral mesh with hexahedral core and prismatic layer. (a) VPC axial flow fan, (b) Sweep axial flow fan.

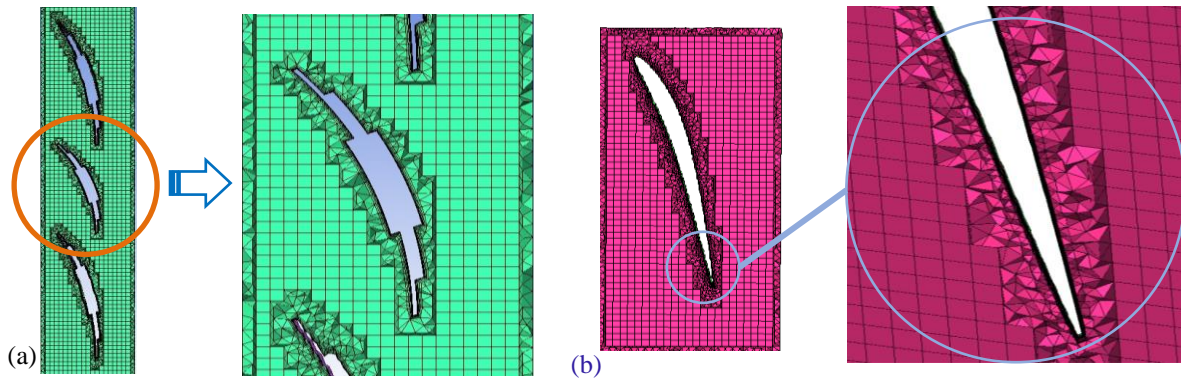


Figure 5. Detail of mesh refinement in the region near the blades. (a) Rotor axial VPC; (b) Rotor axial sweep.

The convergence of the simulations was obtained when the continuity residue is  $1 \times 10^{-5}$ ; and the residues of the velocity, the turbulent kinetic energy and the energy dissipation rate, are equal to the value of  $1 \times 10^{-4}$ . In order to evaluate mesh convergence, the criterion of the percentage difference between the global magnitudes of the refined, coarse and reference meshes was used, which are smaller than 1%. For mesh independence preliminary simulations were considered for the design point of a sweep fan, since the mesh parameters for all types of axial rotors analyzed are similar.

Table II presents the results considered for the mesh independence study. Three meshes were considered. A reference mesh, M, a coarse mesh, M1, and a refined mesh, M2. It can be seen the percentage differences of global quantities such as total pressure,  $\Delta p_T$ , and efficiency,  $\eta$ , with respect to the reference mesh are less than 1%.

Table II. Mesh Independence Parameters

Mesh	No. Elements	$\Delta p_T$ Pa	$\eta$ %
M	10 388 286	120,79	79,03
M1	6 305 072	120,55	78,53
M2	11 091 617	119,69	78,88

### 3.2 Definition of the boundary conditions

As condições de contorno impostas nas superfícies do domínio para a simulação em regime permanente, apresentadas na Figura 2, são as seguintes:

- *Inlet*: the velocity condition was considered, considering initial manometric pressure of 0 Pa, turbulence intensity level of 5% and hydraulic diameter of 0.5 m.
- *Outlet*: the outflow condition is considered. When using this type of condition, it is not necessary to establish pressure or velocity at the fan outlet.
- *Walls*: the non-slip condition, which must be satisfied on the walls, is taken into account. This condition is used in the solid regions where the fluid flows. For the hub and blades was considered the option of rotational movement in relation to the adjacent cell zone (1800 rpm). For another surfaces the stationary wall option is considered.

### 3.3 Discretization and interpolation schemes

To obtain the approximate numerical solutions of the complete Navier-Stokes equations, methods based on discretization techniques of differential flow equations are used. To obtain the pressure and velocity fields, it has been used the *SIMPLE* algorithm (*Semi Implicit Method for Pressure-Linked Equations*), where there is an iterative process based on a relationship between velocity and pressure corrections, thus reinforcing the conservation of mass and obtaining then the pressure field.

For pressure interpolation, the Second Order scheme is used, in which pressure values on cell faces are interpolated using coefficients of the momentum equation.

The second order scheme is used for the numerical solution of the equations of momentum, turbulent kinetic energy and specific dissipation rate.

#### 4. RESULTS OF AERODYNAMIC NUMERICAL ANALYSIS

Through the numerical simulations performed in this work, the results of the aerodynamic characteristics of the 10 axial rotors were obtained, using the post processing tools of the Fluent® program. As for the flow field analysis, static pressure contours, turbulent intensity contours and streamlines were obtained for the maximum efficiency point of the VPC rotor and the Sweep rotor with better aerodynamic behavior.

##### 4.1 Global aerodynamic quantities

From the numerical simulations were obtained the aerodynamic performance curves of the axial flow fans VPC and the 9 sweep geometries. Figure 6 shows the variation of total pressure, hydraulic power and efficiency, respectively, as a function of the flow rate. The values of variation of total pressure, hydraulic power and efficiency of *Sw1* fan (cubic function type 1) are slightly lower with respect to fan VPC values; however the flow rate reaches the 3 m<sup>3</sup>/s. The *Sw2* fan (cubic function type 2), has values of aerodynamic quantities lower than the values of the VPC fan. The geometry *Sw3* with cubic function of type 3 presents a more robust performance, being that the values of variation of total pressure as a function of the flow rate are superior compared with the VPC fan and the flow rate reaches up to 3,75 m<sup>3</sup>/s. The fan *Sw4*, being a variation of the fan *Sw3*, with the modification in the constant distribution of the chord and the thickness from the base to the tip, presents an even more robust performance, since it presents superior total pressure values for a greater flow rate. The *Sw5*, *Sw6*, *Sw7*, *Sw73* e *Sw7310* fans (with cubic function type 4), with variation in the hub ratio, the thicknesses and flow chords, present a slightly more robust performance compared them with the *Sw4* fan.

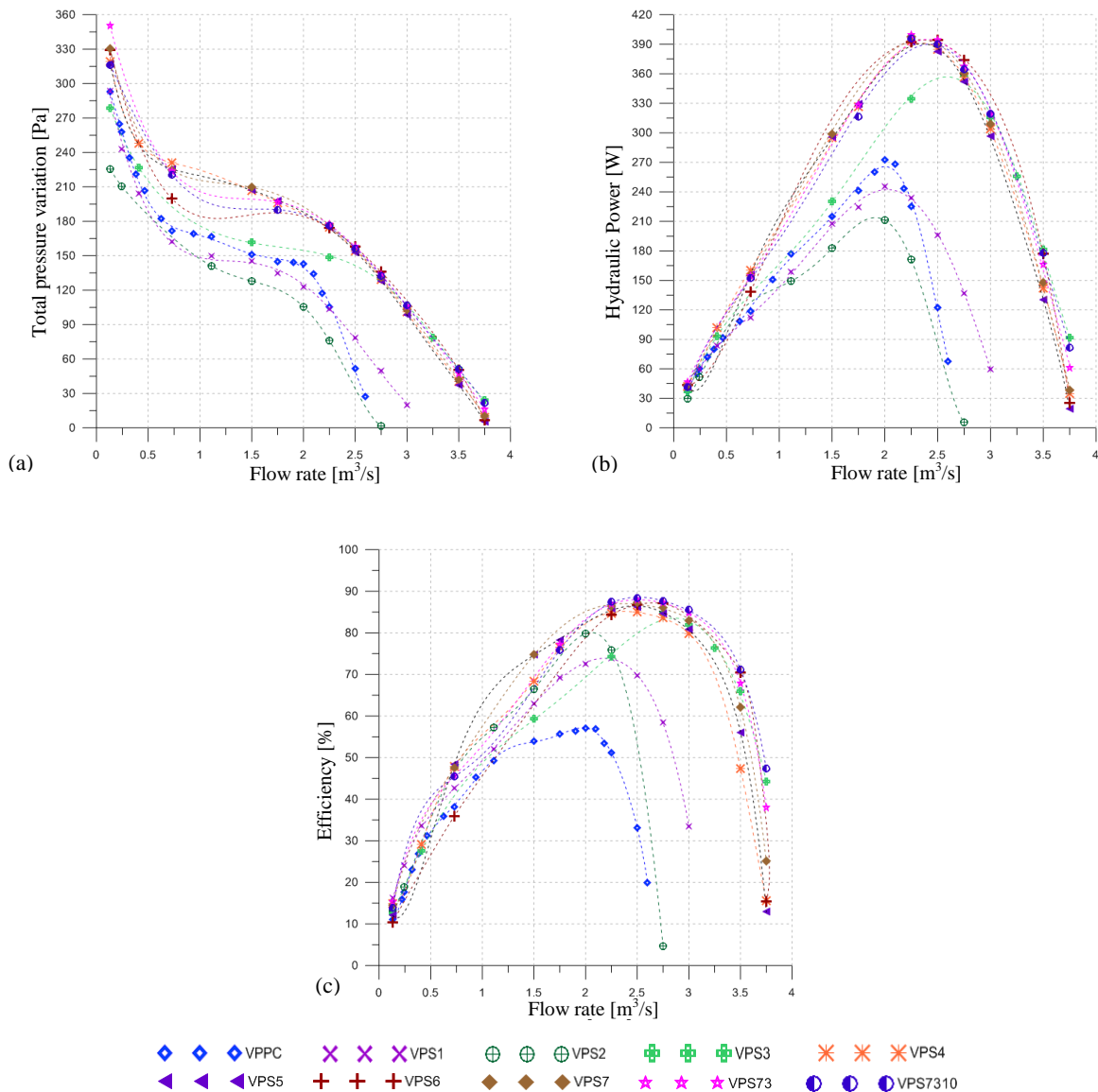


Figure 6. Aerodynamic performance curves of fans: a) total pressure variation; b) Hydraulic power; c) Efficiency.

Table III shows the flow,  $Q$ , and total pressure values,  $\Delta p_T$ , corresponding to the best point efficiency (BEP) of each rotor.

Table III. Flow rate and total pressure values at BEP

Geometria –	$Q$ m <sup>3</sup> /s	$\Delta p_T$ Pa	$\eta$ %
VPC	2,00	143,14	57%
Sw1	2,25	103,81	73,85
Sw2	2,00	105,59	79,85
Sw3	2,75	130,12	84,70
Sw4	2,50	153,92	85,03
Sw5	2,50	153,07	86,22
Sw6	2,75	135,94	87,05
Sw7	2,50	156,20	87,20
Sw73	2,50	157,67	87,92
Sw7310	2,50	155,88	88,26

Since the BEP of the sweep blade fans are close to the design point,  $Q = 1.9 \text{ m}^3/\text{s}$  and  $\Delta p_T = 137.34 \text{ Pa}$ .

It is evident that the sweep axial flow rotors perform better compared to the curved flat blade fan, VPC. The axial flow rotor of curved flat blades has a maximum efficiency of 57%, while sweep axial rotor blades designed for the same operating conditions have maximum efficiencies in the range of 73.85% to 88.26%.

In the analysis of aerodynamic behavior, it is observed that the *Sw7310* geometry presents a better aerodynamic behavior compared to the other geometries.

#### 4.2 Local aerodynamic quantities

Since the behavior of the local flow fields in the sweep rotors are similar, the results corresponding to the *Sw7310* rotor will be analyzed and compared to the results of the VPC curved flat blade rotor.

Figure 7 (a) shows the static pressure contours on the axial rotor of the curved flat blade fan, VPC. The separation of the boundary layers showing the static pressure contours on the ventilator can be identified, causing negative pressure regions.

Figure 7 (b) shows the static pressure contours of the suction side of the *Sw7310* rotor blade. It can be observed that the negative pressure regions in the blade tip decreases considerably compared to conventional axial fan rotors.

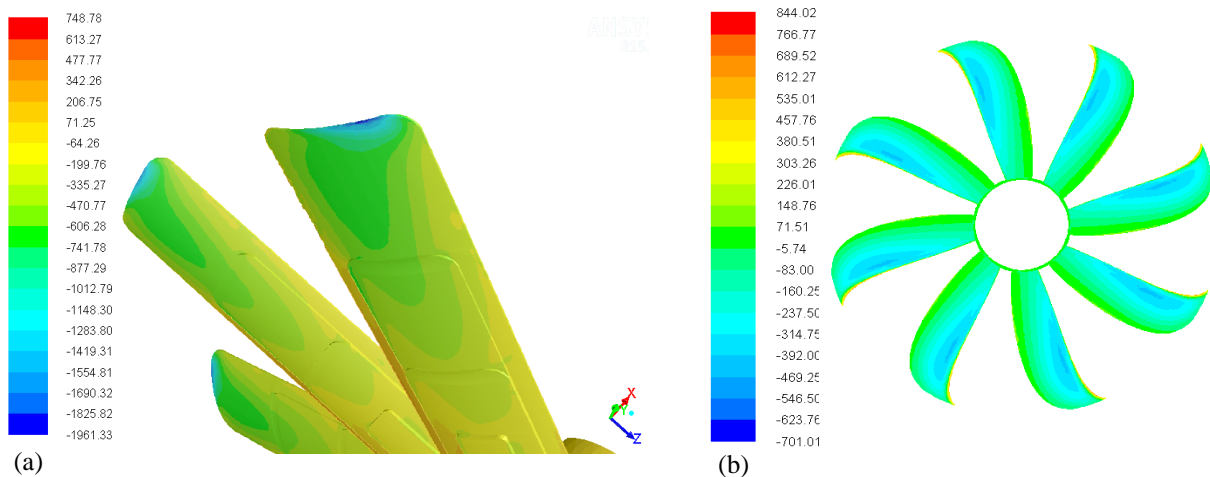


Figure 7. Static pressure contours. (a) VPC fan rotor blades (b) Sw7310 fan suction side.

Figure 8 shows the blade tip vortex of the VPC and Sw7310 rotors resulting from the pressure difference between pressure side and blade suction causing disruption of the downstream rotor flow.

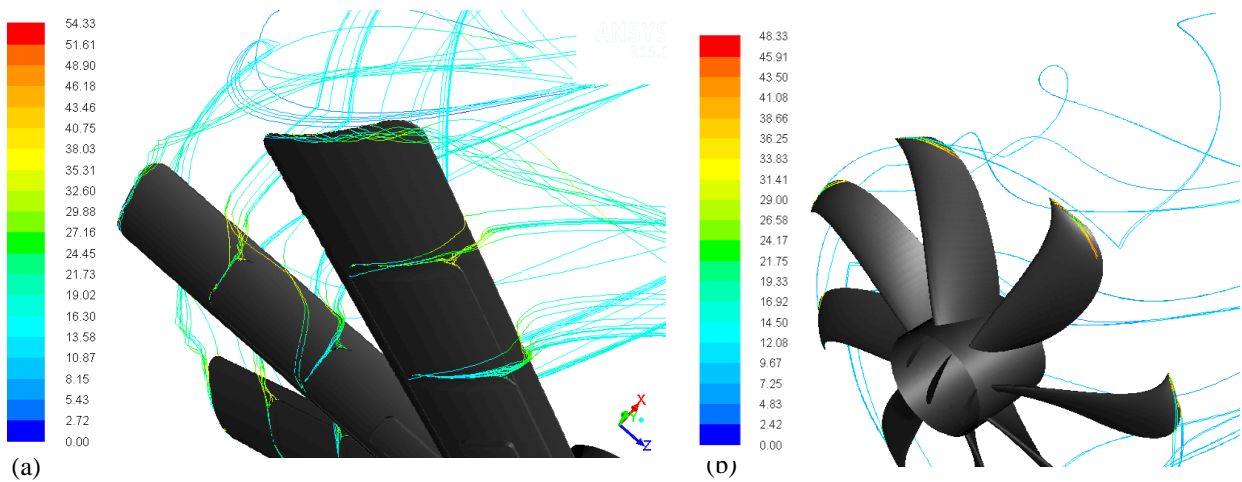


Figure 8. Blade tip vortex. (a) VPC rotor; (b) Sw7310 fan rotor.

In Figures 9 and 10, the contours of the turbulent intensity in the cross section to the axis of rotation of the axial rotors are shown. In Figure 9 the cut in half of the rotor is shown, and in Figure 10 the cut corresponding to the rotor outlet (downstream of the trailing edge). In both geometry, the areas of greatest turbulence indicated by the turbulent intensity were given specifically in the top clearance in the region near the blade tip. However, it can be seen that the VPC axial rotor has its maximum values, in a range between 68% and 85%. The *Sw7310* rotor has its maximum values in a range between 15% and 19%.

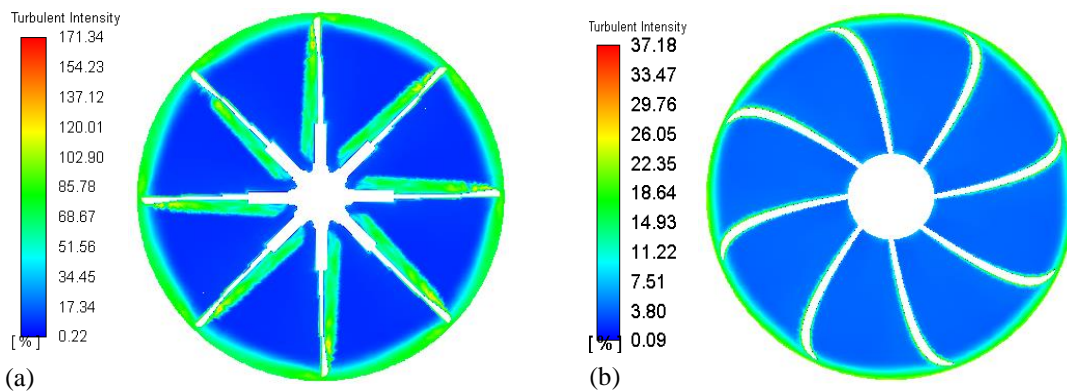


Figure 9. Turbulent intensity contours in cross-section planes on half of rotor. (a) VPC rotor; (b) Sw7310 rotor.

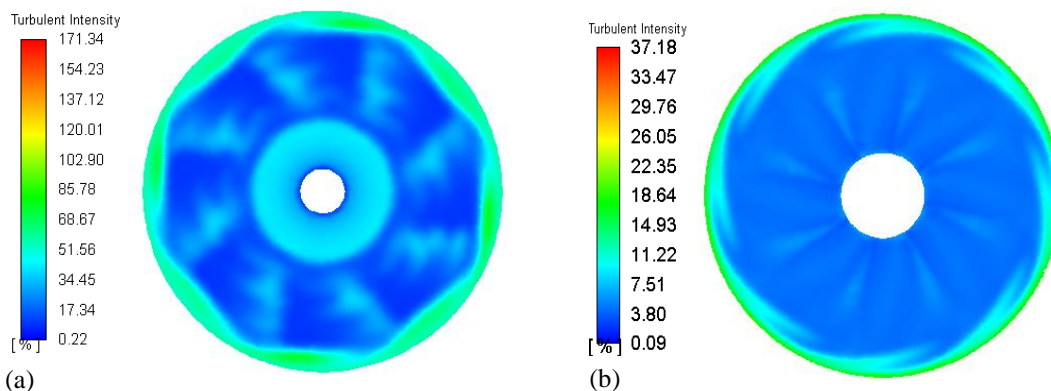


Figure 10. Turbulent intensity contours at rotor output. (a) VPC rotor; (b) Sw7310 rotor.

In Figure 9 (a), it can be seen that the most turbulent intensity zones are in the region of the suction side of the blade and in the region near the tip of the blade of the VPC rotor. In Figure 9 (b), the areas with higher turbulent intensity are more concentrated in the region near the tip of the blade, and in the regions of the pressure and suction side have minimal regions of turbulent intensity.

In Figure 10, it can be seen that the turbulent intensity regions at the rotor output begin to dissipate, but the turbulent intensity of the VPC rotor has a larger range between 51% and 68%, while the Sw7310 rotor has a range between 11 % and 14%.

## 5. CONCLUSIONS

Aerodynamic behavior analyzes of 10 geometries were performed corresponding to the axial flow rotors of fans with different geometric configurations, being 1 fan of flat curved blades and 9 axial rotors with forward sweep.

The sweep rotor geometries were obtained based on the variation of the parameters of the guiding curve that defines the center line of each blade, the hub ratio, and the variation of the chord and thickness from the base to the tip of the blade.

Sweep fan rotors generally exhibit robust aerodynamic behavior in terms of efficiency and total pressure variation, since maximum efficiency values are far from the stall region.

Thus, based on the analysis performed, it can be concluded that the geometry that presents the best aerodynamic behavior was the geometry of the Sw7310 rotor, with a 0.24 hub ratio. The efficiency of this axial rotor being 88.26%.

It is important to highlight that the design point is very close to the maximum efficiency points of the analyzed sweep rotor geometries, which indicates that the adopted methodology is adequate.

## 6. ACKNOWLEDGEMENTS

The authors thank CAPES (Coordenação de Aperfeiçoamento de Pessoal de Nível Superior) for their financial support.

## 7. REFERENCES

- Albuquerque R. B. F., 2006. Teoria da asa de sustentação aplicada às máquinas de fluxo. UNIFEI-IEM, 24p.
- Augustyn O. P. H., 2013. Experimental and Numerical Analysis of Axial Flow Fans. Master thesis, Faculty of Engineering at Stellenbosch University, South Africa.
- Kwedikha, A. R., 2009. Aerodynamic effects of blade sweep and skew applied to rotors of axial flow turbomachinery. Ph. D. thesis, Budapest University of Technology and Economics Faculty of Mechanical Engineering Department of Fluid Mechanics. Budapest, 2009
- Masi M., Lazzaretto A., Stefano Castegnaro S., 2018. "EFFECTIVENESS OF BLADE FORWARD SWEEP IN A SMALL INDUSTRIAL TUBE-AXIAL FAN". In *Proceedings of the International Conference on Fan Noise, Aerodynamics, Applications and Systems- Fan2018*. Darmstadt, Germany.
- Ohtsuta, K.; Akishita, S., 1990. Noise reduction of shortly ducted fans by using forward swept and inclined blades. AIAA-Paper 90-3986.
- VAD, J., 2011. Blade Sweep Applied To Axial Flow Fan Rotors of Controlled Vortex Design. Ph.D. thesis Hungarian Academy of Sciences. Budapest.
- Wright T., Simmons W. E., 1989. "Blade Sweep for Low-Speed Axial Fans". ASME Proceedings digital collection. Journal of Turbomachinery, Volume 112, Issue 1, pp. 151-158.

## 8. RESPONSIBILITY NOTICE

The authors are the only responsible for the printed material included in this paper.